Journal of Applied Physics ARTICLE scitation.org/journal/jap

Theoretical models of spin-exchange optical pumping: Revisited and reconciled

Cite as: J. Appl. Phys. **129**, 154901 (2021); doi: 10.1063/5.0037440
Submitted: 13 November 2020 · Accepted: 28 March 2021 ·
Published Online: 19 April 2021

Michele Kelley and Rosa Tamara Branca[a)]

AFFILIATIONS

Department of Physics and Astronomy, University of North Carolina—Chapel Hill, Chapel Hill, North Carolina 27514, USA

[a)]**Author to whom correspondence should be addressed:** rtbranca@unc.edu

ABSTRACT

Theoretical models for continuous-flow and stopped-flow spin-exchange optical pumping of ^{129}Xe have long predicted much higher ^{129}Xe polarization values than are measured experimentally, leading to a search for additional depolarization mechanisms. In this work, we show that a misapplication of the general theory of spin-exchange optical pumping along with the incorrect use of previously measured spin-exchange constants has been perpetuated in the past 20 years and is the main cause of the long-held discrepancy between theoretical and experimental ^{129}Xe polarization values. Following the standard theory of spin-exchange optical pumping developed almost 40 years ago by Happer *et al.*, we outline the common mistake made in the application of this theory in modern theoretical models and derive a simplified expression of the spin-exchange cross section that can be used to correctly predict ^{129}Xe polarization values under any set of experimental conditions. We show that the complete expression of the spin-exchange cross section derived using the work of Happer *et al.* predicts spin-exchange rates tenfold higher than those previously assumed in theoretical models of continuous-flow and stopped-flow spin-exchange optical pumping and can fully rectify the long-standing discrepancy between theoretical and experimental polarization values.

I. INTRODUCTION

Nuclear spin hyperpolarization is used to increase the sensitivity of nuclear magnetic resonance (NMR) measurements by several orders of magnitude. For a nuclear spin 1/2, hyperpolarization consists of bringing the nuclear spin system out of thermal equilibrium, depopulating one of the two energy states in favor of the other, thus creating a difference in populations between the two energy levels far greater than what is dictated by the Boltzmann distribution at thermal equilibrium. This way, the nuclear polarization, on which the NMR signal depends, becomes magnetic field independent, enabling studies at lower magnetic field strengths or the detection of low-density spin systems like gases.[1–3]

Hyperpolarization of noble gases such as ^{3}He and ^{129}Xe has been used extensively in the last 15–20 years to probe lung ventilation function.[4–6] In recent years, the ability to obtain high levels of ^{129}Xe polarization has enabled studies that go beyond gas-phase imaging.[7–10] Because of its inert nature, high solubility, and large electron cloud, which results in a chemical shift range 20 times larger than other nuclei typically detected in magnetic resonance experiments, hyperpolarized ^{129}Xe has enabled direct detection of gas exchange processes in the lung, brain and kidney perfusion, and tissue temperature.[11–15] For these novel biomedical imaging applications, higher levels of ^{129}Xe polarization and the ability to produce large volumes of gas on short time scales are crucial.

Hyperpolarized (HP) ^{129}Xe is produced via spin-exchange optical pumping (SEOP) with one of two methods, either stopped-flow, where HP ^{129}Xe is produced in a large single batch, or continuous-flow, where HP ^{129}Xe is gradually collected cryogenically until the desired volume is accumulated. Under optical pumping, the valence electrons of an alkali metal vapor, typically Rb, develop a bulk polarization. Optical pumping occurs in a magnetic field where selection rules dictated by the absorption of circularly polarized photons lead to a depopulation of one of the electron spin states and to a bulk electron spin polarization. Then, through spin-exchanging interactions, the electronic spin polarization is transferred to the nuclear spins of ^{129}Xe. Therefore, the final ^{129}Xe polarization depends on several key factors: the Rb polarization, the rate of spin-exchange between Rb and Xe, and the Xe spin-destruction rate, that is the rate at which the nuclear spin system returns back to thermal equilibrium. The final ^{129}Xe

polarization also depends on the Rb vapor density in two ways: the Rb polarization, due to the balance of available photons per Rb atom, and the spin-exchange rate, which is proportional to the Rb vapor density.

Since its advent, the general SEOP theory developed by Happer *et al.*[16–20] has been adapted to predict experimental ^{129}Xe polarization values obtainable under stopped-flow and continuous-flow production of HP ^{129}Xe. For continuous-flow SEOP setups, in particular, these theoretical models have long predicted ^{129}Xe polarization values 2–3 times higher than those achieved experimentally. Previous works attempting to resolve this discrepancy between theoretical and experimental ^{129}Xe polarization values have focused on identifying possible spin-destruction mechanisms.[21–24]

More recently, a re-evaluation of some of the assumptions commonly made in these theoretical models for predicting HP ^{129}Xe polarization values revealed major issues with the way the standard theory of SEOP[19] has been applied in these models.[4,21,23,25–28] Specifically, simulated and experimental Rb vapor densities for continuous-flow SEOP were found to be an order of magnitude smaller than those expected in a closed cell at thermal equilibrium which have been assumed in these models. More interestingly, when correct Rb vapor densities were used in these SEOP models, theoretical ^{129}Xe polarization values fell well below those achieved experimentally, even when considering optimal polarization conditions, pointing out possible additional mistakes in the application of the standard SEOP theory in these models.[29]

Here, by performing an in-depth literature review of the general theory of spin-exchange optical pumping, we reveal a common mistake made in the application of this theory to both continuous-flow and stopped-flow SEOP models. Specifically, we show that a misuse of a simplified expression of the spin-exchange cross section used in SEOP theoretical models, along with the overestimation of the Rb vapor density previously found, led to the long-standing discrepancy between theoretical and experimental ^{129}Xe polarization values. A new expression for the spin-exchange cross section is then derived directly from the standard theory of SEOP, which is then confirmed experimentally. The newly derived expression, along with the true Rb vapor density, is then used to correctly predict experimental ^{129}Xe polarization values.

II. THEORY OF SPIN-EXCHANGE OPTICAL PUMPING

In the following, we summarize the general theory of SEOP that was initially developed by Happer *et al.*,[16–20] to point out the mistakes made in previous papers[4,21,23,25–29] when applying this theory, and to derive an explicit expression of the spin-exchange cross section that can be used in these theoretical models under any set of experimental conditions. For convenience, all constants that appear in this paper and their definitions can be found in the supplementary material.

Under optical pumping, circularly polarized photons are used to spin-polarize the valence electrons of alkali metal atoms, typically a Rb vapor, which acquire a bulk spin polarization. This polarization is then transferred, via the hyperfine interaction, to the nuclear spins of noble gas atoms, such as Xe.

There are two mechanisms that can mediate spin-exchange between a noble gas atom and an alkali metal atom: binary collisions and the formation and destruction of van der Waals molecules. The Hamiltonian for spin exchange through binary collisions can be written as

$$H_{bc} = \alpha \vec{K} \cdot \vec{S}, \tag{1}$$

which describes the isotropic magnetic dipole interaction between the nuclear spin K of the noble gas atom and the electron spin S of the alkali metal atom. As the lifetime of the binary collision, τ_{bc}, is very short ($\approx 10^{-12}$ s), only the nuclear spin of the noble gas atom and the electronic spin of the alkali atom couple. This interaction is typically expressed in terms of a velocity-averaged binary spin-exchange cross section, $\langle \sigma v \rangle$,

$$\langle \sigma v \rangle = \frac{1}{2[\mathrm{Rb}]} \frac{1}{T_{K,bc}} \left(\frac{\alpha \tau_{bc}}{\hbar} \right)^2, \tag{2}$$

where [Rb] is the Rb vapor density, $1/T_{K,bc}$ is the binary collision rate per Xe molecule, α is the coupling constant between K and S, and $\hbar$ is the reduced Planck constant, i.e., the Planck constant divided by 2π.

Spin exchange during the lifetime of a loosely bound van der Waals molecule is more complex. This is because a three-body collision must first occur to form the van der Waals molecule and then another three-body collision must occur to break up the molecule. During the lifetime of the van der Waals molecule, τ, and at low field strengths, the hyperfine interaction dominates the Zeeman interaction and the spin-dependent part of the Hamiltonian can be approximated by

$$H_{vdw} = A \vec{I} \cdot \vec{S} + \gamma \vec{N} \cdot \vec{S} + \alpha \vec{K} \cdot \vec{S}, \tag{3}$$

where $A\vec{I} \cdot \vec{S}$ represents the isotropic magnetic dipole interaction between the alkali nuclear spin I and the electron spin S, $\gamma \vec{N} \cdot \vec{S}$ represents the spin-rotation interaction—this term contributes to spin destruction as the electron spin angular momentum is transferred to the rotational angular momentum N of the molecule—and $\alpha \vec{K} \cdot \vec{S}$ represents the isotropic magnetic dipole interaction between the nuclear spin K of the noble gas atom and the electronic spin S of the alkali atom.

Because under normal SEOP conditions ($B_0 \approx 20$ G) A^2 is much greater than both γ^2 and α^2, we can still use the atomic quantum number $F = I + S$ of the alkali atom to define the energy levels of the van der Waals molecule. Additionally, we can define two helpful parameters,

$$x = \frac{\gamma N}{\alpha} \tag{4}$$

and

$$\phi = \frac{\gamma N \tau}{\hbar} = \frac{p_{o,i}[T]}{p_i}. \tag{5}$$

The parameter x is known as the Breit–Rabi field parameter and it

describes the fraction of the alkali spin S that is transferred to the rotational angular momentum N of the van der Waals molecule vs that transferred to the nuclear spin K of the noble gas atom. Therefore, x, or better its inverse, is a measure of the spin-transfer efficiency between the alkali metal and the noble gas atoms.[30] Its value was found to be 4.1 for ^{129}Xe-Rb by Bhaskar *et al.*[31] The parameter ϕ represents the angle of rotation of S about N and its expression implicitly assumes that the dephasing of S occurs during the entire lifetime of the van der Waals molecule.[19,32,33] ϕ can be expressed in terms of the characteristic pressure p_o, which is temperature dependent, and the pressure of the gas, p.[17,34]

For the molecular Hamiltonian, we can define two distinct regimes. The first is referred to as the short lifetime regime where both

$$\begin{aligned} \frac{\gamma N\tau}{\hbar} &\ll 1, \\ \frac{\alpha\tau}{\hbar} &\ll 1, \end{aligned} \tag{6}$$

but the lifetime of the van der Waals molecule is sufficiently long such that I and S are still strongly coupled together and F is a good quantum number, that is,

$$\frac{A(2I+1)\tau}{2\hbar} \gg 1. \tag{7}$$

Under these conditions, the only allowed transitions are those that occur with a change in the atomic quantum number f associated with F of $\Delta f = 0$. We can then express the fraction of the interactions that can be described by the short lifetime regime, also known as the f-dampening regime, as[18]

$$f_f = \sum_i \frac{\eta_i \left(\frac{A(2I_i+1)\tau}{2\hbar}\right)^2}{1+\left(\frac{A(2I_i+1)\tau}{2\hbar}\right)^2} = \sum_i \frac{\eta_i(\omega_{hf,i}\tau)^2}{1+(\omega_{hf,i}\tau)^2}, \tag{8}$$

where η is the abundance of each alkali isotope and ω_{hf} is the hyperfine frequency of the isotope.

In the regime where Eq. (6) still holds but

$$\frac{A(2I+1)\tau}{2\hbar} \ll 1, \tag{9}$$

the molecular lifetime is so short that I and S cannot couple to F. In this regime, referred to as the very-short molecular lifetime regime, or s-dampening regime, transitions can occur with a change in the atomic quantum number of $\Delta f = 0, \pm 1$.[18,19] The fraction of s-dampening interactions can be expressed as

$$f_s = \sum_i \frac{\eta_i}{1+\left(\frac{A(2I_i+1)\tau}{2\hbar}\right)^2} = \sum_i \frac{\eta_i}{1+(\omega_{hf,i}\tau)^2}. \tag{10}$$

By using the above analytical expressions for the fraction of spin-exchanging interactions in the short and very-short lifetime regimes, we can write a general expression (which is nothing but a weighted average) for the rate of change in the nuclear spin polarization of the noble gas atom $\langle K_Z\rangle$ under SEOP,

$$\begin{aligned} \frac{d}{dt}\langle K_Z\rangle = &\sum_i \frac{\eta_i(\omega_{hf,i}\tau)^2}{1+(\omega_{hf,i}\tau)^2}\frac{1}{T_K}\left(\frac{\alpha\tau}{(2I_i+1)\hbar}\right)^2 \\ &\times\left(\langle K^2-K_Z^2\rangle\langle F_{Z,i}\rangle - \langle F_i^2-F_{Z,i}^2\rangle\langle K_Z\rangle\right) \\ &+\frac{\eta_i}{1+(\omega_{hf,i}\tau)^2}\frac{1}{T_K}\left(\frac{\alpha\tau}{\hbar}\right)^2\left(\langle K^2-K_Z^2\rangle\langle S_Z\rangle - \langle S^2-S_Z^2\rangle\langle K_Z\rangle\right) \\ &+\frac{1}{T_{K,bc}}\left(\frac{\alpha\tau_{bc}}{\hbar}\right)^2\left(\langle K^2-K_Z^2\rangle\langle S_Z\rangle - \langle S^2-S_Z^2\rangle\langle K_Z\rangle\right) - \Gamma\langle K_Z\rangle. \end{aligned} \tag{11}$$

In the above expression, $1/T_K$ is the formation rate of van der Waals molecules, τ is the lifetime of the van der Waals molecule, and Γ is the intrinsic nuclear spin relaxation rate of the noble gas atom.[19] In this equation, the first and second terms represent the van der Waals spin-exchange contributions from the short and very-short lifetime regimes, respectively, whereas the third term represents the contribution from binary collisions. The final term represents the nuclear spin relaxation of the noble gas atom in the absence of an alkali metal vapor. The primary contributors to this term are noble gas–noble gas interactions and wall relaxation. In the very low pressure limit where $f_s \to 0$, the second term in Eq. (11) goes to zero and one recovers the expression that is valid only for the short lifetime regime. If the pressure is increased such that $f_s \to 1$, the first term instead goes to zero and the expression reduces to that valid for the very-short lifetime regime. A weighted average is used in the intermediate regime where contributions from the short and very-short lifetime regimes are expected.

Note that the first term, which describes the contribution from short-lived van der Waals molecules, depends on the total (nuclear and electronic) spin F_Z of the alkali atom, whereas the second term, which describes the contribution from very short-lived van der Waals molecules, depends only on the electronic spin of the alkali atom, S_Z, similar to the term from binary collisions. Equation (11) is a general expression for the rate of change of the nuclear spin of a noble gas atom during spin exchange and can be applied to any alkali–noble gas spin pair. For ^{3}He, which does not participate in the formation of van der Waals molecules, the first two terms are zero and the last term is dominated by wall collisions.

For alkali metals and for noble gas atoms with a nuclear spin of 1/2 like ^{129}Xe, we can easily evaluate some of the expectation values in Eq. (11). For example,

$$\langle S^2-S_Z^2\rangle = \langle K^2-K_Z^2\rangle = \frac{1}{2}. \tag{12}$$

For noble gas atoms with nuclear spins $K > 1/2$, this expectation value will depend on the nuclear spin polarization and will always be greater than 1/2. Likewise, for $F > 1/2$, the expectation value of $\langle F_i^2 - F_{Z,i}^2\rangle$ depends on the alkali metal polarization and can be

written as[19]

$$\langle F_i^2 - F_{Z,i}^2 \rangle = \langle S^2 - S_Z^2 \rangle + \langle I_i^2 - I_{Z,i}^2 \rangle = \frac{1}{2} + I_i(I_i+1) - \frac{1}{\bar{Z}_i}\frac{d^2\bar{Z}_i}{d\beta^2}, \tag{13}$$

where $\bar{Z}$ is the partition function,

$$\bar{Z} = \sum_{m_l=-l}^{l} e^{m_l\beta}, \tag{14}$$

and the constant β represents the spin temperature where

$$P_{\mathrm{Rb}} = \frac{\langle F_Z \rangle}{\langle F^2 - F_Z^2 \rangle} = \frac{\langle I_Z \rangle}{\langle I^2 - I_Z^2 \rangle} = 2\langle S_Z \rangle = \tanh\left(\frac{\beta}{2}\right). \tag{15}$$

Note that the condition for a distribution of Rb states that can be characterized by a Boltzmann spin temperature is satisfied under optical pumping where the radiative lifetimes of optically excited Rb atoms are long compared to Rb-Rb spin-exchange rates, which allows for the mixing of states. A notable exception is found near the optical cell walls where the lifetimes of the excited Rb atoms are severely decreased. In this case, the Rb polarization goes to zero.[35,36] This means we can write

$$\langle F_Z \rangle = 2\langle F^2 - F_Z^2 \rangle \langle S_Z \rangle. \tag{16}$$

Using Eqs. (2), (12), (13), and (16), Eq. (11) becomes

$$\begin{aligned}\frac{d}{dt}\langle K_Z \rangle = \frac{1}{T_K}\left(\frac{\alpha\tau}{\hbar}\right)^2 \Bigg(\sum_i \frac{\eta_i(\omega_{hf,i}\tau)^2}{1+(\omega_{hf,i}\tau)^2} \frac{\langle F_i^2 - F_{Z,i}^2 \rangle}{(2I_i+1)^2} (\langle S_Z \rangle - \langle K_Z \rangle) \\ + \frac{1}{2}\left(\frac{\eta_i}{1+(\omega_{hf,i}\tau)^2}\right)(\langle S_Z \rangle - \langle K_Z \rangle)\Bigg) + [\mathrm{Rb}]\langle \sigma v \rangle (\langle S_Z \rangle \\ - \langle K_Z \rangle) - \Gamma \langle K_Z \rangle.\end{aligned} \tag{17}$$

Furthermore, we must derive an explicit form of the coefficients $1/T_K$ and $\alpha\tau/\hbar$. In order to do this, we can write down an equation describing the chemical equilibrium of the creation and destruction of van der Waals,

$$\begin{aligned}[\mathrm{Rb}] + [^{129}\mathrm{Xe}] + [\mathrm{Xe}] + [\mathrm{He}] + [\mathrm{N_2}] \\ \rightleftharpoons [\mathrm{Rb} - ^{129}\mathrm{Xe}] + [\mathrm{Xe}] + [\mathrm{He}] + [\mathrm{N_2}].\end{aligned} \tag{18}$$

By using T_K, the van der Waals formation time constant, and τ, the break-up time constant, and assuming equilibrium, we can write

$$\begin{aligned}\frac{[^{129}\mathrm{Xe}]}{T_K} = \frac{[\mathrm{Rb} - ^{129}\mathrm{Xe}]}{\tau} \\ = Z_{\mathrm{Xe}}[\mathrm{Rb}][^{129}\mathrm{Xe}][\mathrm{Xe}] + Z_{\mathrm{He}}[\mathrm{Rb}][^{129}\mathrm{Xe}][\mathrm{He}] \\ + Z_{\mathrm{N_2}}[\mathrm{Rb}][^{129}\mathrm{Xe}][\mathrm{N_2}],\end{aligned} \tag{19}$$

where Z_i is the molecular formation rate per unit volume, which sets the magnitude of the spin-transfer rate.[30]

Additionally, we can define an equilibrium constant,

$$\kappa = \frac{[\mathrm{Rb} - ^{129}\mathrm{Xe}]}{[\mathrm{Rb}][^{129}\mathrm{Xe}]} = \frac{[\mathrm{Rb} - \mathrm{Xe}]}{[\mathrm{Rb}][\mathrm{Xe}]}, \tag{20}$$

which has been found to have a $T^{-3/2}$ temperature dependence.[34] This constant also implies that the van der Waals molecules form with no isotopic preference. Rearranging Eq. (19),

$$\frac{\tau^2}{T_K} = \frac{\kappa^2[\mathrm{Rb}]}{Z_{\mathrm{Xe}}[\mathrm{Xe}] + Z_{\mathrm{He}}[\mathrm{He}] + Z_{\mathrm{N_2}}[\mathrm{N_2}]}, \tag{21}$$

and by defining a new constant,

$$\gamma_M = \frac{\alpha^2\kappa^2}{Z_{\mathrm{Xe}}\hbar^2}, \tag{22}$$

one can finally write

$$\frac{1}{T_k}\left(\frac{\alpha\tau}{\hbar}\right)^2 = \frac{\gamma_M[\mathrm{Rb}]}{[\mathrm{Xe}] + \frac{Z_{\mathrm{He}}}{Z_{\mathrm{Xe}}}[\mathrm{He}] + \frac{Z_{\mathrm{N_2}}}{Z_{\mathrm{Xe}}}[\mathrm{N_2}]}. \tag{23}$$

The terms $Z_{\mathrm{He}}/Z_{\mathrm{Xe}}$ and $Z_{\mathrm{N_2}}/Z_{\mathrm{Xe}}$ are equal to $p_o(Xe)/p_o(He)$ and $p_o(Xe)/p_o(N_2)$, respectively, where p_o is defined in Eq. (5). These terms are typically expressed as b_{He} and $b_{\mathrm{N_2}}$. Note that as we have defined γ_M in terms of Xe, $b_{\mathrm{Xe}} = 1$. Using these expressions and considering that for noble gas atoms with nuclear spin 1/2, $P_{\mathrm{Xe}} = 2\langle K_Z \rangle$, and that for alkali atoms like Rb, $P_{\mathrm{Rb}} = 2\langle S_Z \rangle$,

$$\begin{aligned}\frac{d}{dt}\langle P_{\mathrm{Xe}} \rangle = \Bigg(\frac{\gamma_M[\mathrm{Rb}]}{[\mathrm{Xe}] + b_{\mathrm{He}}[\mathrm{He}] + b_{\mathrm{N_2}}[\mathrm{N_2}]} \\ \times \left(\sum_i \frac{\eta_i(\omega_{hf,i}\tau)^2}{1+(\omega_{hf,i}\tau)^2} \frac{\langle F_i^2 - F_{Z,i}^2 \rangle}{(2I_i+1)^2} + \frac{1}{2}\left(\frac{\eta_i}{1+(\omega_{hf,i}\tau)^2}\right)\right) \\ + [\mathrm{Rb}]\langle \sigma v \rangle \Bigg)(\langle P_{\mathrm{Rb}} \rangle - \langle P_{\mathrm{Xe}} \rangle) - \Gamma \langle P_{\mathrm{Xe}} \rangle.\end{aligned} \tag{24}$$

Thus, the total spin-exchange cross section[37] σ_{SE} can be written as

$$\begin{aligned}\sigma_{SE} = \frac{\gamma_M}{[\mathrm{Xe}] + b_{\mathrm{He}}[\mathrm{He}] + b_{\mathrm{N_2}}[\mathrm{N_2}]} \\ \times \left(\sum_i \frac{\eta_i(\omega_{hf,i}\tau)^2}{1+(\omega_{hf,i}\tau)^2} \frac{\langle F_i^2 - F_{Z,i}^2 \rangle}{(2I_i+1)^2} + \frac{1}{2}\left(\frac{\eta_i}{1+(\omega_{hf,i}\tau)^2}\right)\right) + \langle \sigma v \rangle,\end{aligned} \tag{25}$$

which leaves $\langle \sigma v \rangle$, γ_M , b_i, and $\omega_{hf}\tau$ as the only constants to be determined experimentally. Measurements of these constants date back to the 1980s and 1990s and have been made mostly under different experimental conditions than are used for current SEOP production of HP ^{129}Xe. In Sec. III, we report a summary of the values found for these constants in the literature.

III. PAST MEASUREMENTS OF SPIN-EXCHANGE CONSTANTS

A. Past measurements of $\langle\sigma v\rangle$

Spin exchange due to binary collisions can be understood through a velocity-averaged spin-exchange cross section, $\langle\sigma v\rangle$, which is independent of constituent gas densities. This cross section has been measured by several groups under different experimental conditions. Table I summarizes the results of these measurements. One of the first measurements of this cross section was done by Cates *et al.* at low field.[38] In this measurement, a Rb vapor density based on the Killian formula was assumed, which has been noted to be inaccurate in these cases.[39–41]

A later measurement of this cross section by Jau *et al.* was done at high field (9.4 T) to suppress the contribution from van der Waals molecules.[42] A 20% increase in this cross section was predicted at low field as compared to their direct measurements at 9.4 T, which is reported in Table I. Unlike previous measurements, Jau *et al.*[42] directly measured the Rb density using Faraday rotation, yielding a seemingly more precise measurement than the earlier measurement by Cates *et al.*[38] It is interesting to compare the value measured by Jau *et al.* (2.18×10^{-22} m^3 s^{-1}) to that measured by Rice and Raftery[43] (0.6×10^{-22} m^3 s^{-1}) who used the Killian formula to estimate the Rb vapor density. Both were done at high field, 9.4 and 4.7 T, respectively. However, while Jau *et al.* stated that high field suppresses the contribution of van der Waals molecules to spin exchange (see Appendix in Ref. 42), Rice and Raftery noted a pressure-dependent term which they attributed to a van der Waals mechanism.

Later, measurements done by Shao[40] at low field (20 G) and with Xe densities below 1 amagat revealed a much higher binary spin-exchange cross section. Like Jau *et al.*, Shao also used Faraday rotation to directly measure the Rb density; however, their low-field measurement led to a cross section four times higher. Nonetheless, if one considers that the use of the Killian formula leads to a 2–3-fold overestimation of the Rb vapor density in closed cells, it does seem that the measurements of Cates *et al.*, Shao *et al.*, and Zeng *et al.*[30] agree. Yet, these measurements assume that wall relaxation is temperature independent, which for HP ^{3}He has been shown to be a poor assumption.[44]

TABLE I. Measurements of velocity-averaged spin-exchange cross section.

Group (year)	$\langle\sigma v\rangle$ (10^{-22} m^3 s^{-1})	Temperature (°C)	Field strength (G)	Pressure (Torr)	[Rb] method
Zeng *et al.*[30] (1985)	4.1	70–110	5	11–101	Killian
Cates *et al.*[38] (1992)	3.7	75–120	0.11	295–1867	Killian
Augustine and Zilm[45] (1997)	2.7/7.4	60–100	23 500	500/1576	Smithells
Jau *et al.*[42] (2002)	2.18	120–200	94 000	≥600	Faraday
Rice and Raftery[43] (2002)	0.6	90–130	47 000	1786	Killian
Shao[40] (2005)	10	110–150	20	176–530	Faraday

B. Past measurements of γ_M

Per its definition in Eq. (22), γ_M is a function of the hyperfine coupling constant α, the equilibrium constant κ, and the Xe molecular formation rate Z_{Xe}. As the averaged hyperfine coupling constant is inversely proportional to the equilibrium constant, $\langle\alpha\rangle \propto 1/\kappa$,[46] the potential temperature dependence of γ_M comes from Z_{Xe}. If we consider that $Z_{Xe} \propto p_o(Xe)$, then we might expect a strong temperature dependence as $p_o(Xe) \propto \tau \propto T^{-2}$ as suggested by Nelson and Walker,[34] and consequently $\gamma_M \propto T^2$. The constant γ_M has been measured by both Cates *et al.*[38] and Shao *et al.*[47] (Table II) but neither of them considered its possible temperature dependence. Here, it is important to emphasize that during these two experiments, all measurements, except Cates' highest pressure one, were made in the short lifetime regime (i.e., $f_s = 0$ and $f_f = 1$). Only under this condition, the expression for the change in ^{129}Xe polarization simplifies to

$$\frac{d}{dt}\langle P_{Xe}\rangle = \left(\frac{\gamma_M[\mathrm{Rb}]}{[\mathrm{Xe}] + b_{He}[\mathrm{He}] + b_{N_2}[\mathrm{N_2}]}\sum_i \eta_i \frac{\langle F_i^2 - F_{Z,i}^2\rangle}{(2I_i+1)^2} + [\mathrm{Rb}]\langle\sigma v\rangle\right) \times \left(\langle P_{Rb}\rangle - \langle P_{Xe}\rangle\right) - \Gamma\langle P_{Xe}\rangle. \quad (26)$$

Furthermore, under this condition (i.e., $f_s = 0$ and $f_f = 1$), a new parameter $\zeta(P_{Rb})$ can be defined,

$$\zeta(P_{Rb}) \equiv \sum_i \eta_i \frac{\langle F_i^2 - F_{Z,i}^2\rangle}{(2I_i+1)^2}. \quad (27)$$

Additionally, the measurements by Cates *et al.* were done by observing the decay of the ^{129}Xe polarization in the absence of optical pumping, which led to Eq. (27) evaluation at its zero Rb polarization limit, $\zeta(P_{Rb} = 0) = 0.1791$. Shao *et al.*, on the other hand, performed their measurements under optical pumping, with a continuous wave technique called adiabatic fast passage akin to an inversion recovery experiment. As such, Shao assumed the high polarization limit for Rb, $\zeta(P_{Rb} = 1) = 0.0949$, but did not specify or appear to measure the Rb polarization to exactly evaluate Eq. (27).

We must also emphasize that for all these measurements involving spin-exchange, having an accurate measurement of the Rb vapor density is of utmost importance. Whereas Shao *et al.* used Faraday rotation for their Rb vapor density measurement,

TABLE II. Measurements of γ_M.

Group (year)	γ_M (10^4 s^{-1})	Pressure (Torr)	Gas mixture	b_{N_2}	[Rb] method
Cates *et al.*[38] (1992)	2.92	295–1876	Xe/N$_2$	0.275	Killian
Shao[40] (2005)	10.2	176–530	Xe/N$_2$	0.275	Faraday

Cates *et al.* used the Killian formula to evaluate Rb vapor densities. In the same work, Shao *et al.* reported that the Killian formula overestimated the Rb vapor density inside their optical cell by a factor of two. Therefore, it would not be unreasonable to assume a similar error in using the Killian formula with the measurement of Cates *et al.*, which would bring the measurements of Cates *et al.* and Shao *et al.* for γ_M and $\langle\sigma v\rangle$ in closer agreement. Finally, we also want to point out that a possible error in b_{N_2} will also be absorbed into γ_M (neither Cates *et al.* nor Shao *et al.* included He in any of their measurements).

C. Past measurements of b_{N_2} and b_{He} and issues with previous application of SEOP theory

The constants $b_{N_2} = p_o(\mathrm{Xe})/p_o(\mathrm{N_2})$ and $b_{He} = p_o(\mathrm{Xe})/p_o(\mathrm{He})$ can be thought of as the relative ability of N_2 and He, as compared to Xe, to form and break up Rb-Xe van der Waals molecules. Some reported values for the characteristic pressure p_o as defined in Eq. (5) can be found in Table III.

Most applications of SEOP theory have chosen to write the first term in Eq. (26), again an equation valid only in the short lifetime regime, as

$$\frac{\gamma_M[\mathrm{Rb}]}{[\mathrm{Xe}] + b_{He}[\mathrm{He}] + b_{N_2}[\mathrm{N_2}]}\zeta(P_{Rb}) = \frac{[\mathrm{Rb}]}{\sum\frac{[G_i]}{\gamma_i}}, \tag{28}$$

where

$$\gamma_i \equiv \frac{\gamma_M}{b_i}\zeta(P_{Rb}). \tag{29}$$

These species-specific rates, γ_i, have been most widely taken as 5230,[38] 17 000,[48] and 5700[30,43] for Xe, He, and N_2, respectively. Based on the standard SEOP theory, there are two main reasons why these species-specific rates cannot be used under most SEOP conditions for which they have been used. First, the use of Eq. (28) assumes that the system is in a very low-density regime where $f_s = 0$ and $f_f = 1$. This is generally not true for most SEOP ^{129}Xe setups which operate at higher densities ($[G] > 0.5$ amg). In most continuous-flow SEOP setups, high gas pressures are used to increase Xe residence times inside the optical pumping cell and in stopped-flow production higher pressures are used to increase final HP ^{129}Xe volumes, both of which are important for efficient production of large quantities of polarized ^{129}Xe needed for biomedical imaging applications. Second, all these values assume zero Rb polarization—$\zeta(P_{Rb} = 0) = 0.1791$ (see note about γ_{He} in Table IV), a correct assumption in Cates' work, but not for most SEOP setups where Rb polarization is closer to 90%.

Again, we wish to emphasize that while the equations used by Cates *et al.* and Shao *et al.* derive from a correct application of the standard theory of SEOP to their specific experimental setup, these equations [Eqs. (26) and (27)] are not applicable to most current HP ^{129}Xe production conditions for stopped-flow and continuous-flow and therefore should not be used in theoretical models that aim to predict Xe polarization values. Nonetheless, the use of Eq. (26) with $\zeta(P_{Rb} = 0) = 0.1791$ has become standard in the field to evaluate theoretical ^{129}Xe polarization values under higher densities ($[G] > 0.5$ amg) and under optical pumping[4,23,27,28] and, in our opinion, this is the primary cause for the discrepancy between theoretical and experimental polarization values that have so far been reported.

D. Past measurements of $\omega\tau$ (f_f and f_s)

Following the work by Nelson and Walker,[34] we can define a characteristic density $[G]_1$ by

$$\begin{aligned}\omega_{85}\tau &= \frac{[G]_1}{[G]},\\ \omega_{87}\tau &= 2.25\frac{[G]_1}{[G]},\end{aligned} \tag{30}$$

where $[G]$ is the total gas density and the factor 2.25 accounts for the relative hyperfine frequency of the two Rb isotopes. Again, this parameter describes the fraction of interactions that exist in either the short or very-short lifetime regime which, by Eq. (25), contribute to spin exchange at different rates. To our knowledge, only Nelson and Walker[34] probed the transition from the short lifetime to the very-short lifetime regime for lean Xe gas mixtures (1/1/98; Xe/N_2/He). In their work, they noted a very strong temperature dependence $-[G]_1 = 2.8$ amg at 80 °C and 1.95 amg at 150 °C—with additional

TABLE III. Measurements of characteristic pressures, p_o.

Group (year)	$p_o(Xe)$ (Torr)	$p_o(N_2)$ (Torr)	$p_o(He)$ (Torr)	[Rb] method
Ramsey *et al.*[49] (1983)[a]	23-40	107	175	Smithells
Zeng *et al.*[30] (1985)	...	103	...	Faraday
Cates *et al.*[38] (1992)[b]	$28.3(\frac{349}{T})^{\frac{1}{2}}$	...	...	Killian

[a]p_o(Xe) and p_o(N_2) used previously published data by Volt *et al.*,[50] Bhaskar *et al.*,[51] and Bouchiat *et al.*[33]
[b]Not measured, deduced from other works by Zeng *et al.*[30] and Bouchiat *et al.*[33]

TABLE IV. Species-specific rates, γ_i.

Gas	γ_i (s^{-1})	γ_M (10^4 s^{-1})	b_i	$\zeta(P_{Rb})$
Xe	5230[38]	2.92[38]	1	0.1791
N_2	5700[43]	2.92	0.92[a]	0.1791
He	17 000[48]	2.92	0.31[b]	0.1791

[a]γ_M was taken from Cates *et al.*, where $b_{N2} = 0.275$, Rice and Raftery[43] supposedly extracted $b_{N2} = 0.92$ from the work of Zeng *et al.*,[30] but note that Zeng *et al.* measured $p_o(N_2)$ to be 103, which would not give this value considering the reported p_o(Xe).
[b]γ_{He} was an estimation from the work of Cates *et al.*;[38] we note b_{He} could be interpreted as 0.16 if the high polarization limit is taken (the text[48] is not clear), but this is not how it has long been interpreted.[4,25]

data that can be found in Nelson's dissertation.[34,52] Note that, while the quantity above for $[G]_1$ was specific to their gas mixture, the strong temperature dependence ($\propto T^{-2}$) found for $[G]_1$, thus for τ, should still hold for different gas mixtures.

IV. THEORETICAL EVALUATION OF THE Rb-Xe SPIN-EXCHANGE RATE

The above theoretical derivations clearly show that, under the gas density regime typically used for continuous-flow and stopped-flow SEOP production of hyperpolarized ^{129}Xe ($[G] > 0.5$ amg), one has to consider the full expression of the spin-exchange cross section [Eq. (25)] along with Eqs. (13) and (30) in order to correctly predict ^{129}Xe polarization values under a given set of experimental conditions.

Using our derived expression, we can evaluate the expected spin-exchange cross section using previously measured constants, reported in Table V, and their expected temperature dependence. Because the accuracy with which some of these constants have been measured strongly depends on the Rb density values assumed in the experiment, we have selected those constants for which Rb vapor densities were directly measured in the experiment and due to the discrepancy of the effects of field strength on spin-exchange mechanisms (see Sec. III A), we also chose constants that were measured at low field (≈20 G).

By using Eqs. (13), (25), and (30), we were then able to estimate the value of the spin-exchange cross section under our experimental conditions, which included a gas mixture of 1/10/89 $Xe/N_2/He$ at 110 °C (the temperature at which the optical cell walls were maintained during continuous-flow SEOP) with a total density of 3.38 amg.

V. EXPERIMENTAL MEASUREMENTS OF THE Rb-Xe SPIN-EXCHANGE RATE

Because of the pressure, magnetic field, and temperature dependence of Eq. (25), the extraction of these constants and their dependencies under all possible different experimental conditions becomes an onerous work. However, for the purpose of estimating ^{129}Xe polarization values under specific experimental conditions, great simplifications can be made to the equation to directly evaluate the spin-exchange rate under the specific experimental conditions used in the lab. While thus far we have discussed the importance of not assuming a Rb vapor density based on empirical models, especially for continuous-flow cells, we must now emphasize the importance of using a method that does not make assumptions about the spin-destruction rate, in particular, the wall relaxation, which dominates other intrinsic and extrinsic relaxation mechanisms. Most of the measurements discussed in Sec. III assume that the wall relaxation rate is temperature independent. Yet, for Rb and Rb-K hybrid cells used for HP ^{3}He production, this notion of temperature independent wall relaxation has long been debunked. Various studies have found that ^{3}He wall relaxation rates increase exponentially with temperature and have consequentially introduced an "X-factor" to characterize the wall relaxation of a given cell.[39,53–55] For an in-depth discussion of this issue, we refer the reader to Gentile *et al.*[44] Even if perhaps less important, it would be naïve to think that a similar effect does not exist for ^{129}Xe. Indeed, the very different results found in Tables I–III do indicate a similar "cell-dependent" effect, even when the Rb vapor densities are directly measured.

Therefore, to avoid making any assumptions about wall relaxation, one can take the following approach first used by Chann *et al.* for measuring the spin-exchange rate between Rb and ^{3}He.[39,44] The solution to Eq. (24) can be expressed as

$$P_{\mathrm{Xe}}(t) = \frac{\sigma_{SE}[\mathrm{Rb}]}{\sigma_{SE}[\mathrm{Rb}] + \Gamma} P_{\mathrm{Rb}}\left(1 - e^{-(\sigma_{SE}[\mathrm{Rb}]+\Gamma)t}\right). \tag{31}$$

At times much greater than the spin-up time τ_{OP} given by

$$\tau_{OP} = \frac{1}{\sigma_{SE}[\mathrm{Rb}] + \Gamma}, \tag{32}$$

an equilibrium polarization is reached,

$$P_{\mathrm{Xe}}(t \gg \tau_{OP}) = \sigma_{SE}[\mathrm{Rb}]\tau_{OP}P_{\mathrm{Rb}}. \tag{33}$$

Therefore, if [Rb], τ_{OP}, $P_{\mathrm{Xe}}(t \gg \tau_{OP})$, and P_{Rb} are measured one should be able to extract the total spin-exchange cross section as,

$$\sigma_{SE} = \frac{P_{\mathrm{Xe}}(t \gg \tau_{OP})}{P_{\mathrm{Rb}}[\mathrm{Rb}]\tau_{OP}}. \tag{34}$$

To estimate the spin-exchange cross section under our experimental conditions, we performed a total of 15 experiments during which each of these four parameters ([Rb], τ_{OP}, $P_{\mathrm{Xe}}(t \gg \tau_{OP})$, and P_{Rb}) was measured.

TABLE V. Experimental constants used in theoretical evaluations.

Constant	Value	Source
γ_M	10.2×10^4 s^{-1}	Shao[40]
b_{N2}	$\frac{28.3}{107}(\frac{349}{T})^{1/2}$	Cates *et al.*,[38] Ramsey *et al.*[49]
b_{He}	$\frac{28.3}{175}(\frac{349}{T})^{1/2}$	Cates *et al.*,[38] Ramsey *et al.*[49]
$\langle\sigma v\rangle$	10×10^{-22} m^3 s^{-1}	Shao[40]
$[G]_1$	2.4 amg	This work, based on Nelson and Walker[34]
$[G]$	3.38 amg	This work
P_{Rb}	0.81	This work
η_{85}, η_{87}	0.7215, 0.2785	...
[Xe], [N_2], [He]	0.01[G], 0.1[G], 0.89[G]	This work
f_s	0.56	This work
Γ	0.0045 s^{-1}	This work

A. Measuring [Rb]

The Rb vapor density, [Rb], was measured in the optical cell using optical absorption spectroscopy during each of the 15 experiments performed. According to Beer's Law, the intensity of light

passing through absorbing atoms, here Rb, can be described by

$$I(\nu) = I_o(\nu)e^{-[\mathrm{Rb}]l\sigma}, \tag{35}$$

where I_o is the characteristic line shape of the light source, I is the intensity of the light after passing through the sample of length l, and σ is the absorption cross section. By rearranging Eq. (35) and integrating over the frequency, one can extract the density of Rb as

$$[\mathrm{Rb}] = \frac{1}{\pi r_o c f l}\int ln(\frac{I_o(\nu)}{I(\nu)})d\nu, \tag{36}$$

as by definition,

$$\int \sigma(\nu)d\nu = \pi r_o c f, \tag{37}$$

where r_o is the classical electron radius, c is the speed of light, and f is the oscillator strength of the transition. The absorbance, $\ln(I_o/I)$, can be fitted with the Lorentzian function,

$$L(\nu) = \frac{A + 2\pi T(\nu - \nu_o)}{(\nu - \nu_o)^2 + (\frac{\gamma}{2})^2} + B, \tag{38}$$

where B accounts for physically irrelevant instrumental gains, A and T represent the depth and asymmetry of the peak, respectively, γ is the peak width, and ν_o is the center frequency. The Rb vapor density can then be expressed as

$$[\mathrm{Rb}] = \frac{1}{\pi r_o c f l}\int_{-10\gamma}^{10\gamma} \frac{A + 2\pi T(\nu - \nu_o)}{(\nu - \nu_o)^2 + (\frac{\gamma}{2})^2} d\nu, \tag{39}$$

where the limits of integration were chosen to be 10 times larger than the fitted linewidth, γ. This process was repeated for both the D_1 and D_2 peaks, and the results from the two peaks were then averaged.

For these measurements, a modified oven enclosure was built for our commercial polarizer such that optical absorption measurements could be made perpendicular to the pumping beam. Similar to Couture *et al.*,[56] a broadband halogen lamp was used as the light source. After passing through the optical cell, the light was collected into a fiber optic cable using a 100 mm focal length lens. The fiber optic cable coupled the light into our home-built spectrometer, described in greater detail in Antonacci *et al.*,[21] with a spectral resolution of 0.009 nm/pixel.

The optical cell on our polarizer was closed at room temperature (22 °C) and at a pressure of 3.65 atm to get the most precise measurement of the gas density. These values were chosen because they reproduce the same density of 3.38 amg as 110 °C (the temperature at which the cell walls were maintained during SEOP) and 4.74 atm, which are our standard operating parameters for hyperpolarized ^{129}Xe production. Prior to each measurement the oven, which held the cell walls at 110 °C, and the laser (≈36 W) were turned on and the system was allowed to stabilize as determined by a constant laser transmission value. To measure the Rb density, the laser was briefly turned off and 4599 averages were taken over the course of approximately 2 min. Note that the laser has to be turned off during these measurements as optical pumping leads to emission at the D_2 frequency due to energy-pooling.[57,58] In our system, emission at the D_2 frequency resulted in an ≈25% reduction of the white light absorption at the same frequency and to a significant underestimation of the Rb density when measurements were made during optical pumping (see the supplementary material).

B. Measuring τ_{OP}

A spin-up NMR spectroscopy experiment was used to measure the τ_{OP} of ^{129}Xe during SEOP. To depolarize ^{129}Xe before the spin-up experiment, the field (≈20 G) was turned off for 3 min. This depolarized the Rb vapor, which in turn depolarized ^{129}Xe through spin exchange. The field was then turned on ($t = 0$ s), and a spin-up experiment was started. The ^{129}Xe polarization buildup was then probed every 6 s until $t = 870$ s ($\approx 5\tau_{OP}$) using a small surface coil (≈3 cm in diameter, $Q \approx 23.5$) resonant at 24.7 kHz. A small flip angle was used to not significantly perturb the polarization. The ^{129}Xe signal intensity as a function of time t was then fit to the equation

$$S_{\mathrm{Xe}}(t) = S_{eq}(1 - e^{-\frac{t}{\tau_{OP}}}), \tag{40}$$

where S_{Xe} is the signal amplitude and S_{eq} represents the equilibrium signal amplitude in mV.

C. Measuring $P_{\mathrm{Xe}}(t \gg \tau_{OP})$

The equilibrium polarization of ^{129}Xe is proportional to the asymptotic signal from the τ_{OP} spin-up experiment. In order to convert this signal from mV to absolute polarization values, we used a thermal proton source as typically done.[4,5] Additionally, because our proton calibration was done at room temperature (22 °C), we also accounted for the coil's change in resistance at 110 °C, the temperature at which the ^{129}Xe polarization was measured. Specifically, we measured the coil's resistance at 22 and 110 °C, obtaining 7.8 and 10.1 Ω, respectively. By using the small angle approximation for the tip angle θ used in our spin-up experiments, we can then write the signal induced in the coil as

$$S_{coil} \propto B_1 \sin(\theta) \approx B_1\theta \propto {B_1}^2. \tag{41}$$

On resonance,

$$B_1 \propto I \propto R^{-1}, \tag{42}$$

where I is the current in the coil and R is the coil resistance. The relative magnetization probed by the coil at 110 °C vs at 22 °C can then be written as

$$\frac{S_{22}}{S_{110}} \propto \left(\frac{B_{1,22}}{B_{1,110}}\right)^2 \propto \left(\frac{R_{110}}{R_{22}}\right)^2 = 1.68. \tag{43}$$

This conversion factor, along with the ^{1}H thermal calibration experiment, gave a final calibration constant of 3.63 %/mV.

D. Measuring P_{Rb}

Rb polarization is typically measured using the Faraday rotation method, which requires the use of a far detuned laser and lock-in amplifier, which are not always available and which would further complicate the experimental setup of common continuous-flow polarizers. For this reason, in this study, the Rb polarization was measured using the field cycling method first suggested by Nikolaou *et al.*[59] This method, however, can only be used when Beer's law can still be used to describe the attenuation of the laser light during optical pumping, an assumption that, as will be shown here, is only valid under specific experimental conditions.

The attenuation of the photon flux, ϕ, down the length of the cell is given by

$$\frac{d\phi}{dz} = -[\mathrm{Rb}](1 - P_{\mathrm{Rb}}(z))\gamma_p(z), \tag{44}$$

where γ_p is the optical pumping rate.[36] The optical pumping rate is proportional to the photon flux by the photon absorption coefficient, β,

$$\gamma_p = \beta\phi. \tag{45}$$

Assuming 100% circular polarization, the polarization of Rb is given by

$$P_{\mathrm{Rb}}(z) = \frac{\gamma_p(z)}{\gamma_p(z) + \Gamma_{SD}}, \tag{46}$$

where Γ_{SD} is the spin-destruction rate of Rb. Using Eqs. (44)–(46), the optical pumping rate can be written as

$$\frac{d\gamma_p(z)}{dz} = -\beta[\mathrm{Rb}]\gamma_p(z)\left(1 - \frac{\gamma_p(z)}{\gamma_p(z) + \Gamma_{SD}}\right). \tag{47}$$

If we assume that the Rb density is relatively homogeneous throughout the cell, the solution to this equation becomes

$$\gamma_p(z) = \Gamma_{SD} W\left(\frac{\gamma_p(0)}{\Gamma_{SD}} \exp\left(\frac{\gamma_p(0)}{\Gamma_{SD}} - \beta[\mathrm{Rb}]\right)\right), \tag{48}$$

where W is the Lambert W function. Based on this equation, if

$$\frac{\gamma_p(0)}{\Gamma_{SD}} \gg \beta[\mathrm{Rb}]z, \tag{49}$$

the optical pumping rate and thus the polarization of Rb will be approximately constant along the length of the cell. In this case, the polarization of Rb will decrease linearly with the Rb density. For our measurements that were made at a low Rb density (not optically thick vapor), $\beta[\mathrm{Rb}]z \approx 0.22$, and under optical pumping with a laser of tens of Watts, $\gamma_p(0)/\Gamma_{SD} \geq 10$ away from the cell wall. Under these conditions, $P_{\mathrm{Rb}}(z) = P_{\mathrm{Rb}}$. Combining Eqs. (44) and (45),

$$\frac{d\phi}{dz} = -[\mathrm{Rb}](1 - P_{\mathrm{Rb}})\beta\phi(z), \tag{50}$$

whose solution,

$$\phi(z) = \phi_o \exp(-[\mathrm{Rb}](1 - P_{\mathrm{Rb}})\beta z), \tag{51}$$

is nothing else than Beer's law, where the absorbance, A, is represented by

$$A = [\mathrm{Rb}](1 - P_{\mathrm{Rb}})\beta l = \langle N^+\rangle \beta l, \tag{52}$$

where l is the path length and $\langle N^+\rangle$ is the number density of Rb atoms in the $m_j = 1/2$ state, which is averaged along the main axis of the optical cell. The dependence on only those atoms in the $m_j = 1/2$ state is due to the selective nature of circularly polarized light σ^-. Similar logic can be used for σ^+ light. To summarize, if the Rb density is approximately constant in the cell and Eq. (49) is satisfied, Beer's law can be used to describe the attenuation of light during optical pumping.

In terms of $\langle N^+\rangle$, the average Rb polarization can be written as

$$\langle P_{\mathrm{Rb}}\rangle = \frac{\langle N^+\rangle - \langle N^-\rangle}{\langle N^+\rangle + \langle N^-\rangle}. \tag{53}$$

When the magnetic field is turned off, $P_{\mathrm{Rb}} \approx 0$ and

$$\langle N_0^+\rangle = \langle N_0^-\rangle = \frac{1}{2}(\langle N_0^+\rangle + \langle N_0^-\rangle). \tag{54}$$

This means that we can express the ratio of the absorbance with (A) and without (A_0) the magnetic field as

$$\frac{A}{A_0} = \frac{2\langle N^+\rangle}{\langle N^+\rangle + \langle N^-\rangle}, \tag{55}$$

which we can manipulate in a clever way such that

$$\frac{A}{A_0} - 1 = \frac{2\langle N^+\rangle}{\langle N^+\rangle + \langle N^-\rangle} - \frac{\langle N^+\rangle + \langle N^-\rangle}{\langle N^+\rangle + \langle N^-\rangle} = \frac{\langle N^+\rangle - \langle N^-\rangle}{\langle N^+\rangle + \langle N^-\rangle} = \langle P_{\mathrm{Rb}}\rangle. \tag{56}$$

Then simply,

$$\langle P_{\mathrm{Rb}}\rangle = \left|\frac{A}{A_0} - 1\right|. \tag{57}$$

We can then relate the absorbance to the transmittance, T, and the photodiode voltage with (V) and without (V_c—i.e., for a cool cell) Rb vapor by

$$A = -\ln(T) = -\ln\left(\frac{V}{V_c}\right). \tag{58}$$

In terms of these measured quantities, the average Rb polarization becomes

$$\langle P_{\mathrm{Rb}}\rangle = \left|\frac{\ln\left(\frac{V}{V_c}\right)}{\ln\left(\frac{V_0}{V_c}\right)} - 1\right|, \tag{59}$$

where V_0 is the photodiode voltage in the absence of a magnetic field.

In our experiments, the photodiode voltage (with and without the magnetic field) was measured both before and after our spin-up experiment and the results of these two measurements were averaged together. We should note that these measurements represent an upper limit to the Rb polarization because the laser light does not fully illuminate the cell body and the measurement is averaged over the volume of the cell that is illuminated. Additionally, these measurements do not account for the Rb polarization near the cell walls, which is expected to be close to zero.[36]

The above experiments were performed 15 times over the course of 3 days. After five measurements, the cell was cooled down to room temperature and left overnight.

VI. RESULTS

A. Theoretical results

The spin-exchange cross section, as predicted by Eq. (25), depends on several parameters among which are the Rb polarization, the gas density, and the temperature. These dependencies are shown in Fig. 1 and the Mathematica (Wolfram Research) script used to analyze these dependencies is provided in the supplementary material. To illustrate why it is important to consider both regimes, we plot in Fig. 2 the diverging behavior of the van der Waals spin-exchange cross section obtained by using the species-specific rates, when considering only the short lifetime regime contribution, and when considering the full form of the equation derived herein. This plot is for a gas temperature of 110 °C and a gas composition of 1/10/89 Xe/N_2/He. However, it is important to note that an increase in the temperature only lowers the gas density at which the spin-exchange cross section obtained considering only the short lifetime contribution diverges from the one obtained by considering both the short and very-short lifetime contributions.

When evaluating the theoretical total spin-exchange cross section for our system (3.38 amg of 1/10/89 Xe/N_2/He and cell walls held at 110 °C) using Eq. (25) and constants from Table V we get a total spin-exchange cross section of 3.15×10^{-21} m^3 s^{-1}. On the other hand, if Eq. (28) (species-specific rates) were used along with the commonly used binary cross section values given by Jau *et al.*,[42] as previously done in Norquay *et al.*,[4] Freeman *et al.*,[23] and in Skinner *et al.*,[27] we get a total cross section of only 3.73×10^{-22} m^3 s^{-1}, approximately an order of magnitude smaller.

The model was then used to estimate the spin-exchange cross section under different experimental conditions used by various investigators, three of which used lean Xe gas mixtures similar to ours and one of which used a Xe rich gas mixture. Table VI reports the specific experimental conditions along with the estimated values of the spin-exchange cross section from the previous works.

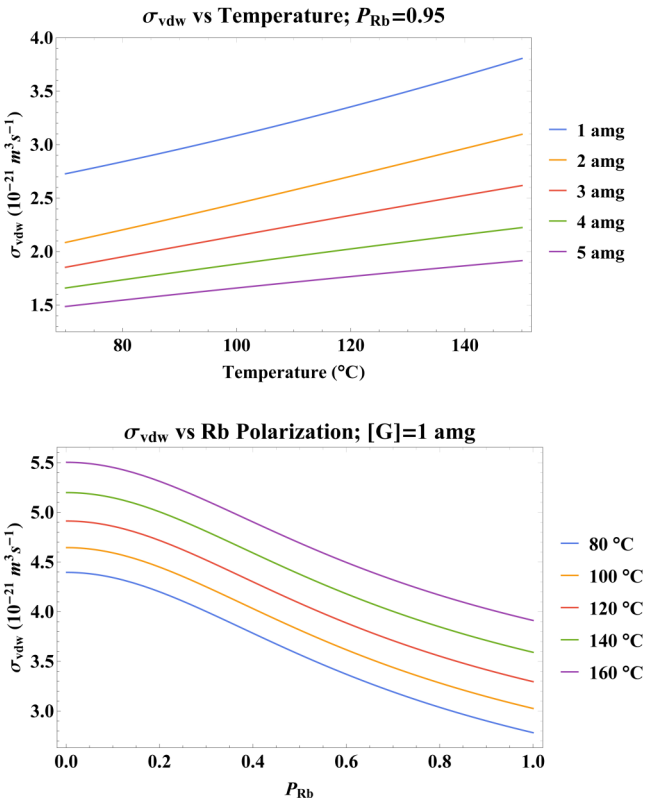

FIG. 1. van der Waals spin-exchange cross section as a function of temperature (top) for various gas densities and for a Rb polarization of 0.95 and as a function of Rb polarization (bottom) for various gas temperatures and for a gas density of 1 amg.

Note that for Hersman *et al.*,[5] Norquay *et al.*,[4] and Freeman *et al.*[23] the value of $[G]_1$ used assumes a gas mixture of 1/1/98 Xe/N_2/He; however, we will assume for these purposes that the majority of He in these mixtures mostly defines the characteristic density $[G]_1$. For these works, we also assumed a 95% Rb polarization as was assumed in Norquay *et al.*[4] but note that this was not explicitly measured.

One of the most interesting cases we found was that of Norquay *et al.*[4] In their work, by using the binary cross section as measured by Jau *et al.*[42] and the species-specific rates, they report a total spin-exchange rate of $[\mathrm{Rb}]\sigma_{SE} = 0.0033\,\mathrm{s}^{-1}$. However, an empirical fit of their data reported in their work led to an estimation of the spin-exchange rate of 0.022 s^{-1}, i.e., an order of magnitude larger than what the species-specific rates [Eq. (28)] predicted. Interestingly, when the correct expression [Eq. (25) with constants from Table V] for the spin-exchange rate is used, one gets a spin-exchange rate of 0.021 s^{-1}. Note that they used the Killian formula to extract a Rb density of 5.82×10^{18} m^{-3} at 100 °C. Another interesting case was that from Skinner *et al.*[27] in which a stopped-flow SEOP setup with a Xe rich gas mixture was used. In Skinner *et al.*, the spin-exchange cross section was

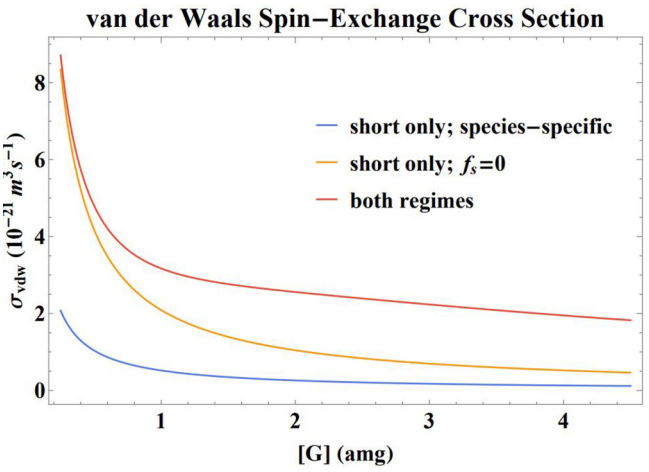

FIG. 2. van der Waals spin-exchange cross section at 110 °C as a function of total gas density evaluated using different models. The blue curve represents the spin-exchange cross section derived from using the species-specific rates, which implicitly assume a zero Rb polarization limit and contributions only from the short lifetime regime. The yellow curve assumes a high Rb polarization limit and constants from Table V, but assumes that all interactions are short lived. The red curve also uses a high Rb polarization limit and the constants from Table V, but considers contributions from both the short and very-short lifetime regimes.

TABLE VI. Theoretical evaluation of σ_{SE} for previous works.

Group (year)	[G] (amg)	Temperature (°C)	f_s	σ_{SE}, original (10^{-21} m^3 s^{-1})	σ_{SE}, Eq. (25) (10^{-21} m^3 s^{-1})
Hersman *et al.*[5] (2008)	0.42	160	0.04	N/A	**3.73**[a]
Norquay *et al.*[4] (2013)	1.44	100	0.20	0.58	**3.69**[b]
Freeman *et al.*[23] (2014)	3.87	150	0.70	0.35	**3.27**[c]
Skinner *et al.*[27] (2020)	2.43	90	0.07	0.30/0.55	**1.51**[d]

[a]Spin-exchange cross sections evaluated using (Eq. 25) are reported in bold font. Because of the large size of the optical pumping cell, high pressures are not needed to extend Xe residence times. Therefore, $f_s \approx 0$ and the simplified form of Eq. (26) can be used.

[b]Norquay *et al.* empirically fitted for what the spin-exchange rate had to be $\gamma_{SE,emp} = 0.022$ s^{-1}. If we use their reported Rb density, 5.82×10^{18} m^{-3} and the new cross section, we get $\gamma_{SE} = 0.021$ s^{-1}.

[c]Freeman *et al.* cited Norquay *et al.*[4] for constants, which we evaluated. The reader should note the order of magnitude difference between the cross section previously used in their work and the one theoretically evaluated here for the same experimental conditions.

[d]Skinner *et al.* used two different models to evaluate the spin-exchange cross section, both of which assume interactions only in the short lifetime regime. It is interesting that the same group[61] measured the spin-exchange cross section under similar conditions (500 Torr Xe, 1500 Torr N_2 at 90 °C), albeit using empirical formulas for estimating [Rb], and found a value of 1.2×10^{-21} m^3 s^{-1}, much closer to the theoretical value of 1.51×10^{-21} m^3 s^{-1} predicted by our closed form expression.

estimated by using the species-specific rates as well as an expression that had previously been used in Cates *et al.*[38] The same spin-exchange cross section, measured earlier by the same group under similar experimental conditions, was found to be 1.2×10^{-21} m^3 s^{-1}, very similar to the value of 1.51×10^{-21} m^3 s^{-1} we found when using our closed form expression. It is important to note that Skinner *et al.* were operating in the short lifetime regime. Specifically, if we assume like in Nelson and Walker[34] that $[G]_1/[G]_o$ is a constant, with $p_o \propto [G]_o$, then

$$[G]_1 \approx 2.8\left(\frac{p_o(\mathrm{He})}{p_o(\mathrm{Xe})}f_{\mathrm{Xe}} + \frac{p_o(\mathrm{He})}{p_o(\mathrm{N_2})}f_{\mathrm{N_2}} + f_{\mathrm{He}}\right)\left(\frac{353}{T}\right)^2, \qquad (60)$$

where f_i is the fraction of species i in the gas mixture. In comparison to continuous-flow setups, the reduction in the He density of Skinner *et al.* leads to a reduction in the contribution to spin exchange from van der Waals molecules as Xe and N_2 are not as efficient as He at forming and breaking up van der Waals molecules.[49]

A similar analysis was performed for two other experimental works reported in the literature. As it can be seen in Table VI, while in Ruset *et al.*[60] the assumption of being in the short lifetime regime (f-dampening) is valid, for Norquay *et al.*[4] and Freeman *et al.*,[23] that assumption is no longer valid as f_s is equal to 0.2 in the former and 0.7 in the latter. Yet, in both cases, the species-specific rates that assume a van der Waals contribution only from the short lifetime regime were used.

B. Experimental results

The results of the spin-exchange cross section measurements can be found in Table VII. For each day, we report the average value of five independent experiments. Across all 3 days, the average spin-exchange cross section was $4.41 \pm 0.28 \times 10^{-21}$ m^3 s^{-1}, after accounting for the relatively high uncertainty in some of the measurements. This value is very close to 3.15×10^{-21} m^3 s^{-1}, which was predicted by our closed form expression evaluated with constants from Table V, especially considering that both values are an order of magnitude larger than those predicted by previous models (3.73×10^{-22} m^3 s^{-1}). Measurements at lower Xe partial pressures could not be performed due to the low sensitivity of the on board NMR spectrometer. Nonetheless, because the characteristic pressure of Xe is considerably lower than that of N_2 and He,[49] a reduction in Xe partial pressure in favor of an increase in the N_2 or He partial pressures is simply expected to push the spin-exchange interactions further into the very-short lifetime regime. On the other hand, at lower total gas pressures, our closed form expression simply reduces to the form first introduced by Cates *et al.*[38] and then used in Shao

TABLE VII. Measurements of the spin-exchange cross section.

Day (No.)	Temperature (°C)	[G] (amg)	P_{Xe} (%)	P_{Rb} (%)	τ_{OP} (s)	Γ (s^{-1})	σ_{SE} (10^{-21} m^3 s^{-1})
1	110	3.38	28.1	80.1	137	0.0048	4.63 ± 0.45
2	110	3.38	28.5	81.5	143	0.0046	4.36 ± 0.56
3	110	3.38	29.5	82.1	153	0.0042	4.23 ± 0.42

et al.,[47] which was correctly derived from the main SEOP theory more than 30 years ago.

We also analyzed how Rb polarization varies as a function of laser transmission and Rb density. In older systems with low power pumping lasers, it is especially important to monitor the Rb polarization. For example, at the front of the optical cell, our laser power is 36 W, however, measured at the back of the cell, without absorbing Rb vapor, the power is only 13 W. This suggests that a large percentage of our laser power is not coupled to the optical cell partially due to reflective losses at the glass window of the oven and the curved glass windows of the optical cell, and partially due to the slight divergence of the laser beam.[4,23] As shown in Fig. 3, the Rb polarization is tightly coupled to both the laser transmission and the Rb density. Where Beer's Law is applicable (see discussion in Sec. V D), the Rb polarization has a logarithmic dependence on the transmission and the Rb density. This may provide a good metric for monitoring the Rb polarization during the production of hyperpolarized Xe, especially in systems like ours with limited laser power.

Using the empirical fit of the Rb polarization as a function of the Rb vapor density, we can plot the expected ^{129}Xe polarization as a function of the Rb vapor density for our low laser power SEOP setup. Figure 4 shows the expected final ^{129}Xe polarization as a function of Rb vapor density assuming a total gas density of 3.38 amg, a temperature of 110 °C, a gas flow rate of 0.75 SLM, and a 300 ml volume optical cell using both the theoretically estimated and the experimentally measured spin-exchange cross section. As it is clear, an optimal Rb vapor density exists for our polarizer, which is approximately equal to 3.3×10^{18} m^{-3}. It is worth noting that this optimal density is close to the average Rb vapor density we found in the cell during its best performance (average 3.1×10^{18} m^{-3}). Additionally, the steep slope of this curve at Rb densities lower than the optimal one explains why optical cells experience a rapid decline in performance at low Rb vapor densities. We also compared ^{129}Xe polarization values predicted by using Eq. (31), using both the spin-exchange cross section evaluated from Eq. (25) and the one measured experimentally, with ^{129}Xe polarization values obtained experimentally on a different cell for three different Rb densities (Fig. 5). In all cases, to estimate ^{129}Xe polarization values, we did not consider the actual distribution of

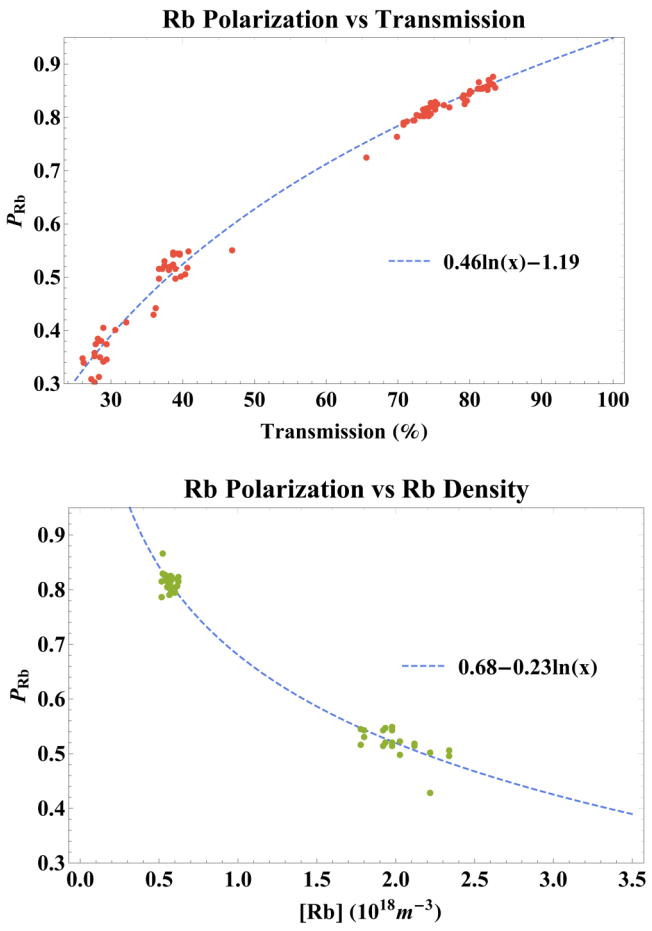

FIG. 3. The Rb polarization as a function of the laser transmission (top) and the Rb polarization as a function of the Rb density (bottom). All data were taken on our small optical cell (≈300 ml) illuminated with a 36 W laser beam. The power measured at the back of the cell without absorbing Rb vapor was 13 W, thus suggesting like in Norquay *et al.*[4] that a large portion of our laser power is not coupled to the optical cell, leading to an overall lower Rb polarization than one might expect. Note that when the Rb polarization drops below ≈70% the assumptions made in Sec. V D do not hold and we expect a larger error.

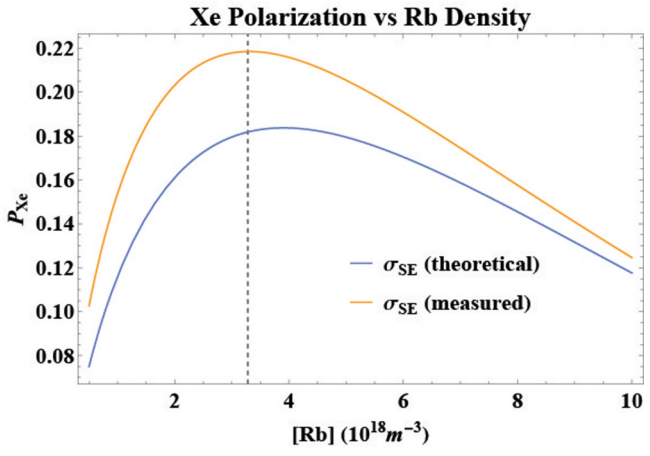

FIG. 4. By evaluating the Rb polarization as a function of density, as found in Fig. 3 and using the measured spin-destruction rate of 0.0045 s^{-1}, one can find the optimal Rb vapor density for a given SEOP system (dashed line). Here, we have assumed a 300 ml optical cell, a gas flow rate of 0.75 SLM, and a residence time given by Eq. (61). The blue curve uses the theoretical spin-exchange cross section obtained using constants from Table V and evaluated for a gas density of 3.38 amg and a temperature of 110 °C. The yellow curve uses the spin-exchange cross section measured experimentally.

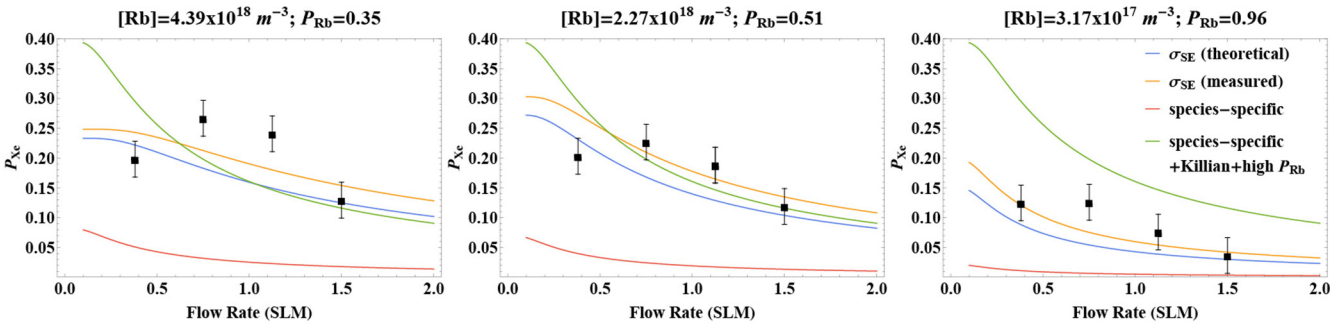

FIG. 5. Experimental data (black) for three different Rb densities and corresponding Rb polarization values acquired on a different cell (2019) than the cell used for the spin-exchange and spin-destruction rate measurements (2020). All theoretical curves (red, blue, yellow, and green) assume the same spin-destruction rate measured experimentally (0.0045 s^{-1}), a cryogenic collection time of 25 min, and a solid state T_1 of 87 min. The green curve assumes a high Rb polarization ($P_{Rb} = 0.96$) as well as a Rb vapor density predicted by the Killian formula ($T = 110\,^{\circ}C$, $[Rb] = 1.09 \times 10^{19}$ m^{-3}) as is routinely done in theoretical models.[4,23]

Xe residence times[29] but simply used the expression

$$t_{res} = \frac{V_{cell}[G]}{Q}, \tag{61}$$

where V_{cell} is the volume of the optical cell in liters and Q is the gas flow rate in standard liters per minute. In Fig. 5, the theoretical yellow curves assume the spin-exchange cross section that was measured for 110 °C, 3.38 amg, and a Rb polarization of 81%; note we have ignored the slight change that a different Rb polarization would make as we expect that 56% of our interactions do not depend on it. The blue curves come from our theoretical analysis [Eq. (25) with values from Table V]. The red curves are for the spin-exchange cross section using the most widely used (but incorrect) species-specific rates and the binary cross section of Jau *et al.*[42] Finally, the green curves again use the species-specific rates and the binary cross section of Jau *et al.* along with a high Rb vapor density (given by the Killian formula) and high Rb polarization ($P_{Rb} = 0.96$) as commonly done in these models. All theoretical curves (yellow, blue, red, and green) assume the same spin-destruction rate, Γ, experimentally measured to be 0.0045 s^{-1}, a cryogenic collection time of 25 min, and a solid state T_1 of 87 min.[4] As seen, while the species-specific rates with the true Rb density and Rb polarization (red) considerably underestimate ^{129}Xe polarization values,[29] theoretical prediction using the theoretically calculated (blue) or experimentally measured (yellow) spin-exchange cross section closely mimics the experimental results.

Finally, our closed form solution for the spin-exchange cross section was used to predict Xe polarization values found in the literature. We pulled data from two works of Nikolaou *et al.*[62,63] where values of the Rb polarization and the Xe spin-destruction rate were measured. For the Rb vapor density, which was not measured, we used the same empirical model used in Skinner *et al.*[27] It is important to point out that in stopped-flow setups a closed cell is heated up to a given temperature, and therefore empirical formulas are expected to provide a reasonable estimation of the Rb vapor density in the cell. For all three data points (shown in Fig. 6), the total pressure of the Xe and N_2 gas mixture was 2000 Torr (2.43 amg) and Eq. (60) was separately evaluated. The degree to which our model is able to predict Xe polarization values across a wide range of Xe partial pressures suggests its robustness and validity.

VII. DISCUSSION

The basic theory of SEOP was developed almost 40 years ago by Happer *et al.*[16–20] While using this theory to predict experimental ^{129}Xe polarization values under continuous-flow and stopped-flow SEOP, several papers have inadvertently made invalid assumptions that led to an apparent discrepancy between

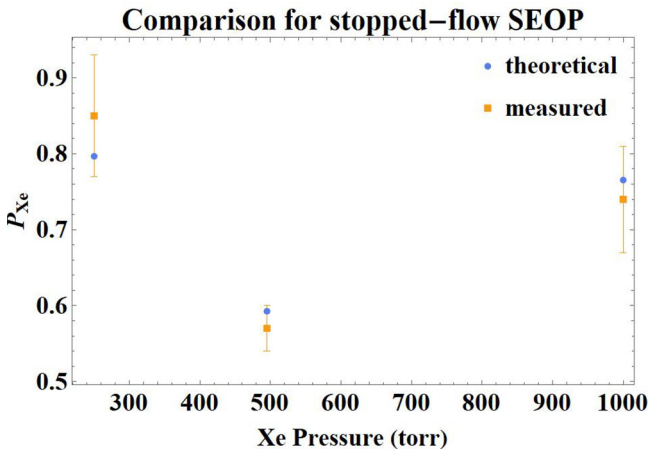

FIG. 6. Comparison between experimentally measured Xe polarization values as a function of Xe partial pressure taken from Nikolaou *et al.*[62,63] and those predicted using our closed form expression for the spin-exchange rate. The total pressure for all data points was 2000 Torr (N_2 buffer). Note that the lowest and highest Xe partial pressure data points correspond to a cell temperature of 62 °C, $P_{Rb} \approx 0.96$, and $\Gamma \approx 1.3 \times 10^{-4}$ s^{-1}, whereas the middle pressure data point corresponds to a cell temperature of 65 °C, $P_{Rb} \approx 0.61$, $\Gamma \approx 1.5 \times 10^{-4}$ s^{-1}.

theoretical and experimental ^{129}Xe polarization values. The first of such assumptions was the use of empirical formulas to estimate the Rb vapor density as discussed in our previous work.[29] Such formulas have been derived for small closed cells, which were thermally equilibrated at a given temperature. While this condition may be close to that found in stopped-flow setups, it is very far from the condition found in continuous-flow setups where cool gas is made to flow atop a pool of hot Rb in an open cell. It is important to point out that these formulas are known to overestimate Rb densities even in closed cells whose walls are not completely coated with a thick layer of Rb.[30,40] The second assumption, discussed here, was the use of a simplified expression for the spin-exchange rate that implicitly assumed a short-lived regime for the van der Waals molecules and a Rb polarization close to zero.

Interestingly, together these two assumptions led to an overestimation of theoretical ^{129}Xe polarization values and to a search for additional depolarization mechanisms. Only recently, the use of Rb vapor densities that had been directly measured for the given setup led to a significant theoretical underestimation of ^{129}Xe polarization values, unveiling additional issues in these models.[29]

In this work, starting from the main theory of SEOP, we have introduced a closed form expression for the spin-exchange cross section that can be used under a variety of different experimental conditions. At the same time, we highlight the mistakes made in previous models in the evaluation of the spin-exchange rate. We show that the spin-exchange cross section assumed in these models considerably underestimated that predicted by the standard SEOP theory. Specifically, models assuming interactions only in the short-lived regime, the conditions under which most of the spin-exchange parameters have been measured, are commonly used to model ^{129}Xe polarization under higher density regimes ($[G] > 0.5$ amg), where contributions not just from short lived, but also from very short-lived van der Waals molecules are to be expected. In doing so, the theoretical spin-exchange rates have been considerably deflated (Fig. 2). This may also explain why models for stopped-flow production of hyperpolarized ^{129}Xe that generally operate at relatively lower pressures have performed much better than those for continuous flow.

Unfortunately, a correct treatment of the van der Waals contribution to spin exchange at higher total gas pressures beyond that found in the fundamental theoretical papers of Happer *et al.*[16–20] cannot be found; all currently used models only consider van der Waals contributions in the short-lifetime regime. Additionally, most of the spin-exchange parameters have been measured under short-lifetime regimes, often acknowledging their possible dependency on both pressure and temperature (Tables I–III). Interestingly, when such parameters are used in the correct expression of the spin-exchange cross section, which includes contributions from both short-lived and very short-lived van der Waals molecules, a much higher spin-exchange cross section is found. These predicted spin-exchange cross sections, which depend on the gas mixture composition, density, and temperature, closely match those empirically derived by other investigators and those directly measured in our experiments (Figs. 5 and 6; Table VI).

Furthermore, when correct Rb densities and spin-exchange cross sections are used in these models, theoretical ^{129}Xe polarization values closely match those obtained experimentally, thus resolving the long-standing discrepancy between theoretical and experimental ^{129}Xe polarization values. Also, the typical overestimation of ^{129}Xe polarization at low flow rates, which has been attributed to laser heating and subsequent Rb runaway,[4] is no longer observed when using the correct spin-exchange rate along with the correct Rb vapor density and Rb polarization (Fig. 5).

The experimental value that we measured for the spin-exchange cross section was $4.41 \pm 0.28 \times 10^{-21}$ m^3 s^{-1} under our operating conditions. As can be seen from Fig. 5, the currently available constants (blue) still slightly underestimate the Xe polarization, thus the true spin-exchange cross section, but are a remarkable improvement over those currently used (red). Also, it is important to note that the Rb polarization measurement is an upper limit on the true value as the Rb polarization was averaged over the volume of the cell that was illuminated. Consequently, the derived spin-exchange cross section and resulting Xe polarization are a lower limit of the true value.

Our work also shows that, in both continuous-flow and stopped-flow SEOP setups, we have an interesting optimization problem that we have summarized in three major takeaways, with the first applying specifically to continuous-flow production. First, the spin-exchange rate decreases with increasing gas density, whereas the residence time, the time during which ^{129}Xe can be polarized, increases with increasing gas density. With small optical cells, the residence time is especially important, which explains the push to higher densities at the cost of a smaller spin-exchange cross section. However, if we consider interactions in both the short and very-short regimes, the spin-exchange cross section does not decrease as severely as it does if only the short regime is considered (Fig. 2). Higher pressures also mean increased Rb absorption through pressure broadening, which could lead to higher Rb polarization depending on the laser profile. Second, to increase the spin-exchange rate, we can increase the temperature, which will have two functions: first to decrease the lifetime of the van der Waals molecules and second to increase the Rb density. Yet, unless there is an excess of laser power, the Rb polarization will start to drop rapidly due to the increased light absorption. This has been observed in our own cell where at a lower density of 5.6×10^{17} m^{-3}, the Rb polarization was approximately 81%, but at a density almost twice that of 2.0×10^{18} m^{-3}, the Rb polarization dropped to 52%. Third, for a given laser power (and flow rate for continuous-flow SEOP), there will be an optimal balance between a high Rb polarization and a high spin-exchange rate. The balance between a high spin-exchange rate and high Rb polarization is why we see a peak in ^{129}Xe polarization at certain transmission or absorption values (see Freeman *et al.*[23] for many examples). This all goes to show why temperature and pressure mapping of the ^{129}Xe polarization is important for optimal performance, but a measure of the Rb vapor density and Rb polarization may be even more important. We wish to emphasize this optimization is most important in systems with limited laser power where the Rb polarization can rapidly decrease due to high absorption. However, this is also seen in high laser power SEOP systems where the final Xe polarization is much greater due to the increased Rb polarization. Indeed, even with 210 W of laser power for a 250 ml optical cell, Zook *et al.* noted an optimal Rb density corresponding to approximately 140 °C, and a decrease in performance at both lower (110 °C) and higher (170 °C) temperatures.[64]

VIII. CONCLUSION

In this paper, starting from the main theory of SEOP developed by Happer *et al.*, we derive a closed form expression for the spin-exchange cross section that can be used from the short to the very-short lifetime regime. While deriving such expression, we point out previous mistakes made in theoretical models that aimed to estimate Xe polarization values in continuous-flow and stopped-flow SEOP setups. Specifically, we show that previous models made invalid assumptions about the molecular lifetime of van der Waals molecules during which spin exchange between alkali metal and noble gas atoms occurs. Specifically, while the use of high gas pressures pushed the system into the very-short lifetime regime, an expression for the spin-exchange rate valid only for the short lifetime regime and in the absence of optical pumping was used. This incorrect assumption, along with an overestimation of the Rb vapor density, led to inflated theoretical ^{129}Xe polarization values that were well above those obtained experimentally and to a search for new ^{129}Xe depolarization mechanisms.

By using the correct Rb vapor density and Rb polarization, and by using the correct expression of the spin-exchange cross section, theoretical ^{129}Xe polarization values closely match those obtained experimentally. As outlined here, improved measurements of spin-exchange theoretical constants are most certainly needed to be able to correctly predict spin-exchange cross sections under each and every experimental condition. However, even though accurate measurements of these parameters do not exist, the proposed closed form expression for the spin-exchange cross section, along with these parameters, can still predict spin-exchange rates close to those we have measured experimentally, which are at least an order of magnitude larger than those previously used in theoretical models.

Clearly, only by using the correct theoretical framework, one can begin to understand and optimize experimental conditions needed to achieve high ^{129}Xe polarization values.

SUPPLEMENTARY MATERIAL

See supplementary material for a complete list of theoretical constants and their definitions used in this work, the Mathematica script that can be used to evaluate the spin-exchange cross section and final ^{129}Xe polarization, and the evidence of Rb energy pooling.

ACKNOWLEDGMENTS

This work was supported by the NIH under Grant Nos. R01DK108231 and R01DK123206, Dr. Branca's startup fund, and the NSF Graduate Research Fellowship (No. DGS1650116.)

DATA AVAILABILITY

The data that support the findings of this study are available within the article and its supplementary material.

REFERENCES

[1]A. M. Coffey, M. L. Truong, and E. Y. Chekmenev, "Low-field MRI can be more sensitive than high-field MRI," J. Magn. Reson. **237**, 169–174 (2013).
[2]W. Shao, G. Wang, F. Raymond, E. Hughes, B. Chronik, G. Scott, S. Conolly, and A. Macovski, "Low readout field magnetic resonance imaging of hyperpolarized xenon and water in a single system," Appl. Phys. Lett. **80**, 2032 (2002).
[3]Y. Zheng, G. D. Cates, W. A. Tobias, J. P. Mugler III, and G. W. Miller, "Very-low-field MRI of laser polarized xenon-129," J. Magn. Reson. **249**, 5108–117 (2014).
[4]G. Norquay, S. R. Parnell, X. Xu, J. Parra-Robles, and J. M. Wild, "Optimized production of hyperpolarized ^{129}Xe at 2 bars for in vivo lung magnetic resonance imaging," J. Appl. Phys. **113**, 044908 (2013).
[5]F. W. Hersman, I. C. Ruset, S. Ketel, I. Muradian, and S. D. Covrig, "Large production system for hyperpolarized ^{129}Xe for human lung imaging studies," Acad. Radiol. **15**, 683–692 (2008).
[6]S. Patz, F. W. Hersman, I. Muradian, M. I. Hrovat, I. C. Ruset, S. Ketel, F. Jacobson, G. P. Topulos, and H. H. J. Butler, "Hyperpolarized ^{129}Xe MRI: A viable functional lung imaging modality?," Eur. J. Radiol. **64**, 335–344 (2008).
[7]M. A. Antonacci, L. Zhang, A. Burant, A. McCallister, and R. T. Branca, "Simple and robust referencing system enables identification of dissolved-phase xenon spectral frequencies," Magn. Reson. Med. **80**, 431–441 (2018).
[8]M. A. Antonacci, C. McHugh, M. Kelley, A. McCallister, S. Degan, and R. T. Branca, "Direct detection of brown adipose tissue thermogenesis in UCP1−/− mice by hyperpolarized ^{129}Xe MR thermometry," Sci. Rep. **9**, 14865 (2019).
[9]M. Rao, N. J. Stewart, G. Norquay, P. D. Griffiths, and J. M. Wild, "High resolution spectroscopy and chemical shift imaging of hyperpolarized ^{129}Xe dissolved in the human brain in vivo at 1.5 tesla," Magn. Reson. Med. **75**, 2227–2234 (2016).
[10]S. Han, H. Kühn, F. W. Häsing, K. Münnemann, B. Blüich, and S. Appelt, "Time resolved spectroscopic NMR imaging using hyperpolarized ^{129}Xe," J. Magn. Reson. **75**, 2227–2234 (2016).
[11]J. Chacon-Caldera, A. Maunder, M. Rao, G. Norquay, O. I. Rodgers, M. Clemence, C. Puddu, L. R. Schad, and J. M. Wild, "Dissolved hyperpolarized Xenon-192 MRI in human kidneys," Magn. Reson. Med. **82**, 262–270 (2020).
[12]G. Norquay, G. Leung, N. J. Stewart, J. Wolber, and J. M. Wild, "^{129}Xe chemical shift in human blood and pulmonary blood oxygenation measurement in humans using hyperpolarized ^{129}Xe NMR," Magn. Reson. Med. **77**, 1399–1408 (2017).
[13]M. R. Rao, N. J. Stewart, P. D. Griffiths, G. Norquay, and J. M. Wild, "Imaging human brain perfusion with inhaled hyperpolarized ^{129}Xe MR imaging," Radiology **286**, 659–665 (2018).
[14]R. T. Branca, T. He, L. Zhang, C. S. Floyd, M. Freeman, C. White, and A. Burant, "Detection of brown adipose tissue and thermogenic activity in mice by hyperpolarized Xenon MRI," Proc. Nat. Acad. Sci. U.S.A. **111**, 18001–18006 (2014).
[15]J. P. Mugler and T. A. Altes, "Hyperpolarized ^{129}Xe MRI of the human lung," J. Magn. Reson. Imaging **37**, 313–331 (2013).
[16]T. G. Walker and W. Happer, "Spin-exchange optical pumping of noble-gas nuclei," Rev. Mod. Phys. **69**, 629–642 (1997).
[17]Z. Wu, T. G. Walker, and W. Happer, "Spin-rotation interaction of noble-gas alkali-metal atom pairs," Phys. Rev. Lett. **54**, 1921–1924 (1985).
[18]S. Appelt, A. Ben-Amar Baranga, C. J. Erickson, M. V. Romalis, A. R. Young, and W. Happer, "Theory of spin-exchange optical pumping of ^{3}He and ^{129}Xe," Phys. Rev. A **58**, 1412 (1998).
[19]W. Happer, E. Miron, S. Schaefer, D. Schreiber, W. A. Van Wijngaarden, and X. Zeng, "Polarization of the nuclear spins of noble-gas atoms by spin exchange with optically pumped alkali-metal atoms," Phys. Rev. A **29**, 3092–3110 (1984).
[20]W. Happer, "Optical pumping," Rev. Mod. Phys. **44**, 170–238 (1972).
[21]M. A. Antonacci, A. Burant, W. Wagner, and R. T. Branca, "Depolarization of nuclear spin polarized ^{129}Xe gas by dark rubidium during spin-exchange optical pumping," J. Magn. Reson. **279**, 60–67 (2017).
[22]C. Flower, M. S. Freeman, M. Plue, and B. Driehuys, "Electron microscopic observations of Rb particles and pitting in ^{129}Xe spin-exchange optical pumping cells," J. Appl. Phys. **122**, 024902 (2017).
[23]M. S. Freeman, K. Emami, and B. Driehuys, "Characterizing and modeling the efficiency limits in large-scale production of hyperpolarized ^{129}Xe," Phys. Rev. A **90**, 023406 (2014).

[24]M. S. Freeman and B. Driehuys, "Hyperpolarized noble gas production systems with nanocluster suppression, detection and/or filtering and related methods and devices," U.S. patent 10,583,205 (March 10, 2020).
[25]I. C. Ruset, "Hyperpolarized ^{129}Xe production and applications, *revised*," Ph.D. thesis (University of New Hampshire, 2007).
[26]J. W. Plummer, K. Emami, A. Dummer, J. C. Woods, L. L. Walkup, and Z. I. Cleveland, "A semi-empirical model to optimize continuous-flow hyperpolarized ^{129}Xe production under practical cryogenic accumulation conditions," J. Magn. Reson. **320**, 106845 (2020).
[27]J. G. Skinner, K. Ranta, N. Whiting, A. M. Coffey, P. Nikolaou, M. S. Rosen, E. Y. Chekmenev, P. G. Morris, M. J. Barlow, and B. M. Goodson, "High Xe density, high photon flux, stopped-flow spin-exchange optical pumping: Simulations versus experiments," J. Magn. Reson. **312**, 106686 (2020).
[28]A. Fink, D. Baumer, and E. Brunner, "Production of hyperpolarized xenon in a static pump cell: Numerical simulations and experiments," Phys. Rev. A **72**, 053411 (2005).
[29]M. Kelley, A. Burant, and R. T. Branca, "Resolving the discrepancy between theoretical and experimental polarization of hyperpolarized ^{129}Xe using numerical simulations and in situ optical spectroscopy," J. Appl. Phys. **128**, 144901 (2020).
[30]X. Zeng, Z. Wu, T. Call, E. Miron, D. Schreiber, and W. Happer, "Experimental determination of the rate constants for spin exchange between optically pumped K, Rb, and Cs atoms and ^{129}Xe nuclei in alkali-metal-noble-gas van der Waals molecules," Phys. Rev. A **31**, 260–278 (1985).
[31]N. D. Bhaskar, W. Happer, and T. McCelland, "Efficiency of spin exchange between rubidium spins and ^{129}Xe nuclei in a gas," Phys. Rev. Lett. **49**, 25–28 (1982).
[32]C. C. Bouchiat, M. A. Bouchiat, and L. C. L. Pottier, "Evidence for Rb-rare-gas molecules from the relaxation of polarized Rb atoms in rare gas—Theory," Phys. Rev. **181**, 144 (1969).
[33]M. A. Bouchiat, J. Brossel, and L. C. Pottier, "Evidence for Rb-rare-gas molecules from the relaxation of polarized Rb atoms in rare gas—Experimental results," J. Chem. Phys. **56**, 3703–3714 (1972).
[34]I. A. Nelson and T. G. Walker, "Rb-Xe spin relaxation in dilute Xe mixtures," Phys. Rev. A **65**, 012712 (2001).
[35]L. W. Anderson and A. T. Ramsey, "Study of the spin-relaxation times and the effects of spin-exchange collisions in an optically oriented sodium vapor," Phys. Rev. **132**, 712 (1963).
[36]S. Appelt, T. Ünlü, K. Zilles, N. J. Shah, S. Baer-Lang, and H. Halling, "Experimental studies of rubidium absolute polarization at high temperatures," Appl. Phys. Lett. **75**, 427–429 (1999).
[37]Note that in keeping with traditional nomenclature, the term cross section should not be used with the formation and destruction of van der Waals molecules. However, here we have adopted it as we are concerned with the total effects of binary collisions and van der Waals.
[38]G. D. Cates, R. J. Fitzgerald, A. S. Barton, P. Bogorad, M. Gatzke, N. R. Newbury, and B. Saam, "Rb-^{129}Xe spin-exchange rates due to binary and three-body collisions at high Xe pressures," Phys. Rev. A **45**, 4631–4639 (1992).
[39]B. Chann, E. Babcock, L. W. Anderson, and T. G. Walker, "Measurements of 3He spin-exchange rates," Phys. Rev. A **66**, 032703 (2002).
[40]W. Shao, "Studies and applications of hyperpolarized ^{129}Xe," Ph.D. thesis (California Institution of Technology, 2004).
[41]Z. Wu, M. Kitano, W. Happer, M. Hou, and J. Daniels, "Optical determination of alkali metal vapor number density using Faraday rotation," Appl. Opt. **25**, 4483 (1986).
[42]Y. Y. Jau, N. N. Kuzma, and W. Happer, "High-field measurement of the ^{129}Xe-Rb spin-exchange rate due to binary collisions," Phys. Rev. A **66**, 052710 (2002).
[43]C. V. Rice and D. Raftery, "Rubidium–xenon spin exchange and relaxation rates measured at high pressure and high magnetic field," J. Chem. Phys. **117**, 5632–5641 (2002).
[44]T. R. Gentile, P. J. Nacher, B. Saam, and T. G. Walker, "Optically polarized ^{3}He," Rev. Mod. Phys. **89**, 045004 (2017).
[45]M. P. Augustine and K. W. Zilm, "Optical pumping magnetic resonance in high magnetic fields: Measurements of high field spin exchange cross sections," Chem. Phys. Lett. **56**, 4569–4578 (1997).
[46]T. G. Walker, "Estimates of spin-exchange parameters for alkali-metalnoble-gas pairs," Phys. Rev. A **40**, 4959–4964 (1989).
[47]W. Shao, G. Wang, and E. W. Hughes, "Measurement of spin-exchange rate constants between ^{129}Xe and alkali metals," Phys. Rev. A **72**, 022713 (2005).
[48]B. Driehuys, G. D. Cates, E. Miron, K. Sauer, D. K. Walter, and W. Happer, "High-volume production of laser-polarized ^{129}Xe," Appl. Phys. Lett. **69**, 10–13 (1996).
[49]N. Ramsey, E. Miron, X. Zeng, and W. Happer, "Formation and breakup rates of RbXe van der Waals molecules in He and N_2 gas," Chem. Phys. Lett. **102**, 340–343 (1983).
[50]C. H. Volk, T. M. Kwon, and J. G. Mark, "Measurement of the ^{87}Rb–^{129}Xe spin-exchange cross section," Phys. Rev. A **21**, 1549–1555 (1980).
[51]N. D. Bhaskar, W. Happer, M. Larsson, and X. Zeng, "Slowing down of rubidium-induced nuclear spin relaxation of ^{129}Xe gas in a magnetic field," Phys. Rev. Lett. **50**, 105–108 (1983).
[52]I. A. Nelson, "Physics of practical spin-exchange optical pumping" Ph.D. thesis (University of Wisconsin-Madison, 2001).
[53]B. Chann, E. Babcock, L. W. Anderson, T. G. Walker, W. C. Chen, T. B. Smith, A. K. Thompson, and T. R. Gentile, "Production of highly polarized ^{3}He using spectrally narrowed diode laser array bars," J. Appl. Phys. **94**, 6908 (2003).
[54]W. C. Chen, T. R. Gentile, T. G. Walker, and E. Babcock, "Spin-exchange optical pumping of ^{3}He with Rb-K mixtures and pure K," Phys Rev. A **75**, 013416 (2007).
[55]B. Lancor and T. G. Walker, "Polarization limits in K-Rb spin-exchange mixtures," Phys. Rev. A **83**, 065401 (2011).
[56]A. H. Couture, T. B. Clegg, and B. Driehuys, "Pressure shifts and broadening of the Cs D1 and D2 lines by He, N_2, and Xe at densities used for optical pumping and spin exchange polarization," J. Appl. Phys. **104**, 4569–4578 (2008).
[57]I. Saha, P. Nikolaou, N. Whiting, and B. M. Goodson, "Characterization of violet emission from Rb optical pumping cells used in laser-polarized xenon NMR experiments," Chem. Phys. Lett. **428**, 268–276 (2006).
[58]M. G. Mortuza, S. Anala, G. E. Pavlovskaya, T. J. Dieken, and T. Meersmann, "Spin-exchange optical pumping of high-density xenon-129," J. Chem. Phys. **118**, 1581 (2003).
[59]P. Nikolaou, N. Whiting, N. A. Eschmann, K. E. Chaffee, B. M. Goodson, and M. J. Barlow, "Generation of laser-polarized xenon using fiber-coupled laser-diode arrays narrowed with integrated volume holographic gratings," J. Magn. Reson. **197**, 249–254 (2009).
[60]I. C. Ruset, S. Ketel, and F. W. Hersman, "Optical pumping system design for large production of hyperpolarized ^{129}Xe," Phys. Rev. Lett. **96**, 053002 (2006).
[61]N. Whiting, P. Nikolaou, N. A. Eschmann, B. M. Goodson, and M. J. Barlow, "Interdependence of in-cell xenon density and temperature during Rb ^{129}Xe spin-exchange optical pumping using VHG-narrowed laser diode arrays," J. Magn. Reson. **208**, 298–304 (2011).
[62]P. Nikolaou *et al.*, "Near-unity nuclear polarization with an open-source ^{129}Xe hyperpolarizer for NMR and MRI," Proc. Nat. Acad. Sci. U.S.A. **110**, 14150 (2013).
[63]P. Nikolaou, A. M. Coffey, L. J. Walkup, B. M. Gust, C. D. LaPierre, E. Koehnemann, M. J. Barlow, M. S. Rosen, B. M. Goodson, and E. Y. Chekmenev, "A 3D-printed high power nuclear spin polarizer," J. Am. Chem. Soc. **136**, 1636–1642 (2014).
[64]A. L. Zook, B. B. Adhyaru, and C. R. Bowers, "High capacity production of >65% spin polarized xenon-129 for NMR spectroscopy and imaging," J. Magn. Reson. **159**, 175–182 (2002).